

Counter-Rotating Accretion Discs

S. Dyda,¹ R.V.E. Lovelace,² G.V. Ustyugova,³ M.M. Romanova,²
& A.V. Koldoba³

¹*Department of Physics, Cornell University, Ithaca, NY 14853; email: sd449@cornell.edu*

²*Department of Astronomy, Cornell University, Ithaca, NY 14853*

³*Keldysh Institute for Applied Mathematics, Moscow, Russia*

22 July 2021

ABSTRACT

Counter-rotating discs can arise from the accretion of a counter-rotating gas cloud onto the surface of an existing co-rotating disc or from the counter-rotating gas moving radially inward to the outer edge of an existing disc. At the interface, the two components mix to produce gas or plasma with zero net angular momentum which tends to free-fall towards the disc center. We discuss high-resolution axisymmetric hydrodynamic simulations of viscous counter-rotating disc for cases where the two components are vertically separated and radially separated. The viscosity is described by an isotropic α -viscosity including all terms in the viscous stress tensor. For the vertically separated components a shear layer forms between them the middle of this layer in free-fall to the disc center. The accretion rates are increased by factors $\sim 10^2 - 10^4$ over that for a conventional disc rotating in one direction with the same viscosity. The vertical width of the shear layer and the accretion rate are strongly dependent on the viscosity and the mass fraction of the counter-rotating gas. In the case of radially separated components where the inner disc co-rotates and the outer disc rotates in the opposite direction, a gap between the two components opens and closes quasi-periodically. The accretion rates are $\gtrsim 25$ times larger than those for a disc rotating in one direction with the same viscosity.

Key words: accretion discs-galaxies: evolution-galaxies:formation-galaxies:nuclei-galaxies:spiral

1 INTRODUCTION

Commonly considered models of accretion discs have gas rotating in one direction with a turbulent viscosity acting to transport angular momentum outward and matter inward. However, observations indicate that there are more complicated, possibly transient, disc structures on a galactic scale. Observations of normal galaxies have revealed co/counter-rotating gas/gas, gas/stars, and stars/stars discs in many galaxies of all morphological types — ellipticals, spirals, and irregulars (Rubin 1994a, 1994b; Galletta 1996; review by Corsini 2014). There is limited evidence of counter-rotating gas components in discs around stars (Remijan and Hollis 2006; Tang et al. 2012). Theory and simulations of co/counter-rotating gas/gas discs predict enormously enhanced accretion rates resulting from the presence of the two components which can give rise to outbursts from these discs (Lovelace and Chou 1996; Kuznetsov et al. 1999;

Nixon, King, and Price 2012; Vorobyov, Lin, and Guedel 2014).

Counter-rotation in disc galaxies appears in a variety of configurations including cases where (1) two cospatial populations of stars rotate in opposite directions, (2) the stars rotate in one direction and the gas rotates in the opposite direction, and (3) two spatially separated gas discs rotate in opposite directions (Corsini 2014). An example of case (1) is the galaxy NGC 4550 which has cospatial counter-rotating stellar discs (Rubin, Graham, and Kenney 1992). Examples of case (2) include the galaxy NGC 3626 (Ciri, Bettoni, and Galletta 1995) and NGC 4546 (Sage and Galletta 1994). An example of case (3) is the “Evil Eye” galaxy NGC 4826 in which the direction of rotation of the gas reverses going from the inner (180 km s^{-1}) to the outer disc (-200 km s^{-1}) with an inward radial accretion speed of more than 100 km s^{-1} in the transition zone, whereas the stars at all radii rotate in the same direction as the gas in

the inner disc, which has a radius of ~ 1200 pc (Braun et al. 1994; Rubin 1994b).

On a stellar mass scale, Remijan and Hollis (2006) and Tang et al. (2012) found evidence of accretion of counter-rotating gas in star forming systems. Accreted counter-rotating matter may encounter an existing co-rotating disc, for example, in low-mass X-ray binary sources where the accreting, magnetized rotating neutron stars are observed to jump between states where they spin up and those where they spin down. Nelson et al. (1997) and Chakrabarty et al. (1997) have proposed that the change from spin-up to spin-down results from a reversal of the angular momentum of the wind-supplied accreting matter.

In the formation of massive black holes in the nuclei of active galaxies, King and Pringle (2006, 2007) argue that in order for the rapid growth of the massive black holes (observed at high red-shifts) to be compatible with the Eddington limit on their emission, the gas accretion is from a sequence clouds with randomly oriented angular momenta. This process would lead to the formation of a disc with the rotation direction alternating as a function of radius.

A number of theoretical and computer simulation studies have explored the different physical processes arising in counter rotating discs. In the case of counter rotating coplanar stellar discs, the two-stream instability is predicted to couple the two components and give rise to low azimuthal mode number ($m = 1, 2$) spiral waves (Lovelace, Jore, & Haynes 1997). N -body simulations of counter rotating stellar discs show a prominent $m = 1$ spiral wave (Comins et al. 1997). The two-stream instability is also important for coplanar stellar/gas discs (Lovelace et al. 1997).

In the case of counter-rotating gas discs, the two components are necessarily spatially separated because otherwise the ensuing strong shocks would destroy the discs. The counter-rotating gas may come from later infall of “new” gas onto a preexisting co-rotating disc. A self-similar analytic solution was derived for accretion discs with isotropic α -viscosity (Shakura and Sunyaev 1973) where the top half of the disc ($Z > 0$) rotates in one direction and the bottom half rotates in the other direction (Lovelace and Chou 1996). The rotation can be Keplerian for accretion to a star or black hole or it can be a flat rotation for the case of a disc galaxy. The gas in the super-sonic shear layer between the two components has nearly free-fall inward radial velocity. The accretion rate is enhanced relative to a conventional disc by a factor of the order of $(R/h)^2 \alpha^{-1/2} \gg 1$, where R is the radius and h is the disc’s half-thickness. The Kelvin-Helmholtz instability is expected to be important in such shear layers. It has been studied earlier in planar supersonic shear layers (Ray 1981, 1982; Choudhury and Lovelace 1983). Gulati, Saini, and Sridhar (2012) studied the $m = 1, 2$ modes component Keplerian discs and found them to be unstable and a possible source of lopsided brightness distributions in galaxies. Using smooth particle hydrodynamic simulations, Nixon et al. (2012) modeled counter-rotating inner and outer AGN discs that were tilted with respect to one another and found that accretion rates could be $\gtrsim 100$ times greater than if they were planar. Also, using smooth particle hydrodynamic simulations, Alig et al. (2013) modeled counter-rotating gas discs with the aim of

explaining the spiral-like filaments of gas feeding the galactic center’s black hole SgrA*.

Spherical grid, axisymmetric hydrodynamic simulations of different configurations of counter-rotating discs were carried out by Kuznetsov et al. (1999). The interaction of the co- and counter-rotating components was mediated by the numerical viscosity. The present work discusses high-resolution axisymmetric hydrodynamic simulations of counter rotating discs including all components of the viscous stress tensor for an isotropic α -viscosity.

Section 2 of the paper discusses the numerical methods and the simulation parameters. Section 3 discusses the simulation results for the cases of vertically and radially separated components. Section 4 gives the conclusions.

2 MODEL

2.1 Basic Equations

The flows are assumed to be described by the equations of non-relativistic hydrodynamics (HD). In a non-rotating reference frame the equations are

$$\frac{\partial \rho}{\partial t} + \nabla \cdot (\rho \mathbf{v}) = 0, \quad (1a)$$

$$\frac{\partial \rho \mathbf{v}}{\partial t} + \nabla \cdot \mathcal{T} = \rho \mathbf{g}, \quad (1b)$$

$$\frac{\partial (\rho S)}{\partial t} + \nabla \cdot (\rho \mathbf{v} S) = \mathcal{Q}. \quad (1c)$$

Here, ρ is the mass density, S is the specific entropy, \mathbf{v} is the flow velocity, \mathcal{T} is the momentum flux density tensor and \mathcal{Q} is the rate of change of entropy per unit volume due to viscous and Ohmic heating in the disc. We assume that the heating is offset by radiative cooling so that $\mathcal{Q} = 0$. Also, $\mathbf{g} = -(GM/r^2) \hat{\mathbf{r}}$ is the gravitational acceleration due to the central mass M . We model the fluid as a non-relativistic ideal gas with equation of state

$$S = \ln \left(\frac{p}{\rho^\gamma} \right), \quad (2)$$

where p is the pressure and $\gamma = 5/3$. We use cylindrical coordinates (R, ϕ, Z) as these are the coordinates used by our code.

The viscosity of the gas is considered to be due to turbulent fluctuations of the velocity. Outside of the disc, the gas is assumed to be ideal with negligible viscosity. The turbulent coefficient is parameterized using the α -model of Shakura and Sunyaev (1973). The turbulent kinematic viscosity is

$$\nu_t = \alpha_\nu \frac{c_s^2}{\Omega_K}, \quad (3)$$

where c_s is the midplane sound speed, Ω_K is the Keplerian angular velocity at the given radii and $\alpha_\nu \leq 1$ is a dimensionless constant.

The momentum flux density tensor is given by

$$\mathcal{T}_{ik} = p \delta_{ik} + \rho v_i v_k + \tau_{ik}, \quad (4)$$

where τ_{ik} is the viscous stress contribution from the turbulent fluctuations of the velocity. As mentioned, we assume

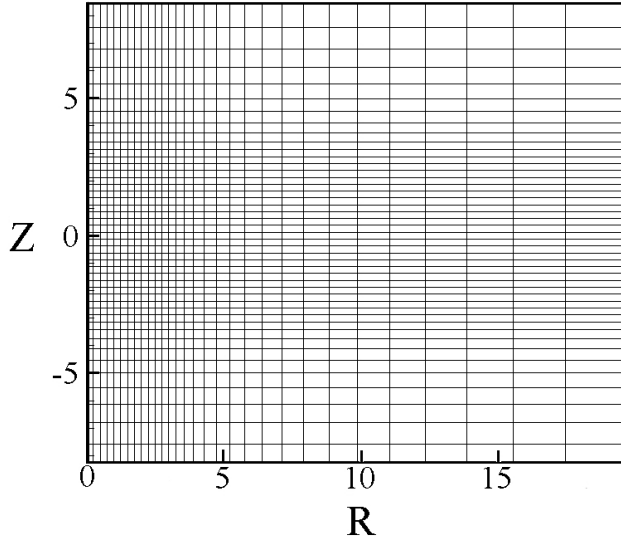


Figure 1. Sparse version of our grid showing 20% of the cells used. The simulations used $N_R \times N_Z = 150 \times 250$ grid cells.

that these can be represented in the same way as the collisional viscosity by substitution of the turbulent viscosity. The leading order contributions to the viscous stress arise from large velocity gradients. In a Keplerian type disc these will be dominated by the azimuthal terms $v_\phi \sim v_K$. However, in a counter-rotating disc the boundary layer between the counter-rotating components experience nearly free fall velocity. Therefore we include all viscous terms involving v_R and v_ϕ . The leading order contribution to the momentum flux density from turbulence are therefore

$$\begin{aligned} \tau_{R\phi} &= -\nu_t \rho R \frac{\partial \Omega}{\partial R}, & \tau_{Z\phi} &= -\nu_t \rho R \frac{\partial \Omega}{\partial Z}, \\ \tau_{ZR} &= -\nu_t \rho \frac{\partial v_R}{\partial Z}, & \tau_{RR} &= -2\nu_t \rho \frac{\partial v_R}{\partial R}, \\ \tau_{\phi\phi} &= -2\nu_t \rho \frac{v_R}{R}, \end{aligned} \quad (5)$$

where $\Omega = v_\phi/R$ is the angular velocity of the gas.

The transition from the viscous disc to the non-viscous corona is handled by multiplying the viscosity by a dimensionless factor $\xi(\rho)$ which varies smoothly from $\xi = 1$ for $\rho \geq \rho_d = 0.75\rho(R, Z=0)$ to $\xi = 0$ for $\rho \leq 0.25\rho_d$ as described in Appendix B of Lii, Romanova, & Lovelace (2012).

2.2 Initial Conditions

2.2.1 Matter Distribution

Initially the matter of the disc and corona are assumed to be in mechanical equilibrium (Romanova et al. 2002). The initial density distribution is taken to be barotropic with

$$\rho(p) = \begin{cases} p/T_{\text{disc}} & p > p_b \text{ and } R \geq R_d, \\ p/T_{\text{cor}} & p < p_b \text{ or } R \leq R_d, \end{cases} \quad (6)$$

where p_b is the level surface of pressure that separates the cold matter of the disc from the hot matter of the corona and R_d is the initial inner disc radius. At this surface the

density has an initial step discontinuity from value p/T_{disc} to p/T_{cor} .

Because the density distribution is barotropic, the initial angular velocity magnitude is a constant on coaxial cylindrical surfaces about the z -axis. Consequently, the pressure can be determined from the Bernoulli equation

$$F(p) + \Phi + \Phi_c = \text{const}, \quad (7)$$

where $\Phi = -GM/\sqrt{R^2 + Z^2}$ is the gravitational potential, $\Phi_c = \int_R^\infty \xi d\xi \omega^2(\xi)$ is the centrifugal potential, and

$$F(p) = \begin{cases} T_{\text{disc}} \ln(p/p_b) & p > p_b \text{ and } R \geq R_d, \\ T_{\text{cor}} \ln(p/p_b) & p < p_b \text{ or } R \leq R_d. \end{cases} \quad (8)$$

The initial half-thickness of the disc h is taken to be $h/R = 0.200$, and the inner disc radius $R_d = 2$. We have also carried out simulations for $h/R = 0.1$ and $R_d = 2$ for the vertically and radially separated components and conclude that the results present below do not depend significantly on h/R in this range.

2.2.2 Angular Velocity

The magnitude of the initial angular velocity is constant along cylinders of constant R . Inside of R_d , the matter rotates rigidly with angular velocity of the star

$$\Omega = (1 - 0.003)\Omega_K(R_d) \quad R \leq R_d. \quad (9)$$

Inside the disc the angular velocity of the disc is slightly sub-Keplerian.

For the simulations of vertically separated co- and counter-rotating components, we consider a positive angular velocity of the lower part of the disc. The upper counter-rotating part of the disc has a negative angular velocity. That is,

$$\Omega = \begin{cases} -(1 - 0.003)\Omega_K(R) & Z > 0 \text{ and } \rho \leq \rho_c, \\ (1 - 0.003)\Omega_K(R) & \text{elsewhere}. \end{cases} \quad (10)$$

We parametrize these runs in terms of the initial ratio of disc mass counter-rotating with the star to the disc mass rotating with the star which we define as Δ . The counter-rotating floor density ρ_c is determined by the choice of Δ .

For the simulations where the co- and counter-rotating components are radially separated at the radius R_c , we consider

$$\Omega = \begin{cases} (1 - 0.003)\Omega_K(R) & R_d < R < R_c, \\ -(1 - 0.003)\Omega_K(R) & R > R_c. \end{cases} \quad (11)$$

2.3 Computational Domain and Boundaries

Our simulation region has three boundaries: the axis, the surface of the star and the external boundaries. For each dynamical variable we impose a boundary condition consistent with our physical assumptions.

We assume axisymmetry. On the star and the external boundaries we impose free boundary conditions $\partial \mathcal{F} / \partial n = 0$ where \mathcal{F} is a dynamical variable and n is the vector normal to the boundary.

The hydrodynamic equations are written in dimensionless form so that the simulation results can be applied to

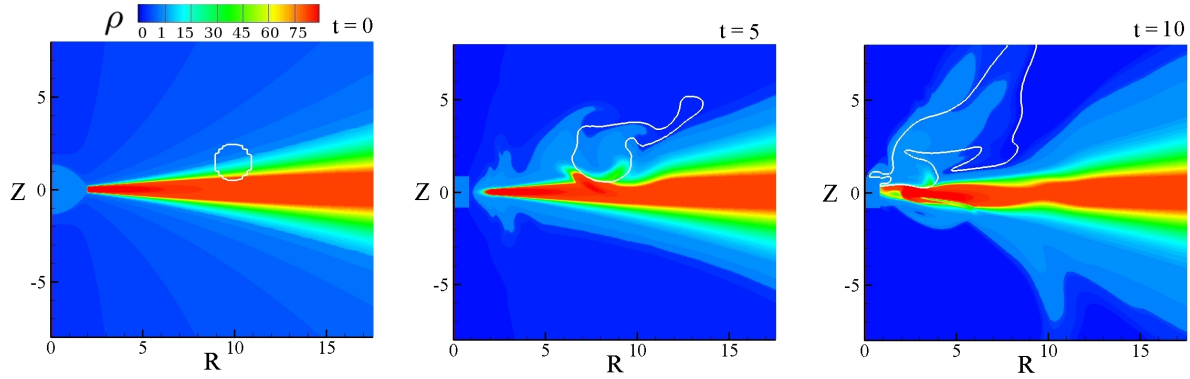


Figure 2. Density ρ (color) and angular velocity $\Omega = 0$ contours (white lines) for $t = 0, 5, 10$ for the torus problem. The initial counter rotating torus (left-hand panel) is observed to free-fall into the star (right-hand panel).

different systems. The mass of the central star is taken as the reference unit of mass, $M_0 = M_\odot$. The reference length, r_0 , is taken to be the radius of the star. The initial inner radius of the disc is $R_d = 2r_0$. The reference value for the velocity is the Keplerian velocity at the radius r_0 , $v_0 = (GM_0/r_0)^{1/2}$. The reference time-scale is the period of rotation at r_0 , $P_0 = 2\pi r_0/v_0$.

At the external boundary along the edge of the disc $-5 < Z < 5$, we allow new matter to flow into the simulation region. We impose the condition that the matter must be accreting $v_R < 0$. In the coronal region, we prescribe outflow conditions and allow matter and entropy to exit the simulation region.

Our simulations use a grid $N_R \times N_Z = 150 \times 250$ cells. The star has a radius of 1 in our dimensionless units and is cylindrical in shape. It extends 10 units above and below the equatorial plane. In the R -direction, the first 60 grid cells have length $dR = 0.05$. At larger radii the cell lengths are given recursively by $dR_{i+1} = 1.025dR_i$. Similarly, in the Z -direction the first 30 grid cells above and below the equatorial plane have length $dZ = 0.05$. At larger Z , the cell lengths are given recursively by $dZ_{j+1} = 1.025dZ_j$. Figure 1 shows a sparse version of our grid with only every 5th cell shown.

3 RESULTS

3.1 Vertically Offset Torus

Here, we consider an equilibrium consisting of a co-rotating disc with a counter-rotating torus of a small amount of mass with major axis R_0 and minor axis $r \ll R_0$ located at (R_0, Z_0) . The mass of the torus is 1% of the disc's total mass, and it is in hydrostatic equilibrium with the disc in the Z -direction. This is for the purpose of modeling the accretion of a counter-rotating cloud onto the surface of a preexisting co-rotating disc. Figure 2 shows the infall of the torus at several times. The torus falls inward over the top surface of the disc towards the star. Even though the torus has a very small mass fraction it induces axisymmetric warping of the disc. When it reaches the star it gives a large spike in the stellar accretion rate \dot{M}_* as shown in Fig. 3.

The infall time of the torus from R_0 to the star,

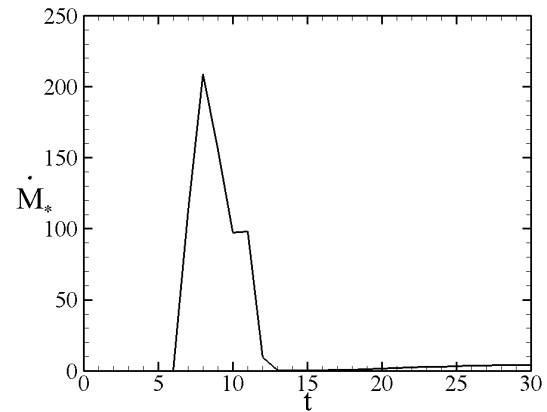


Figure 3. Mass accretion rate to the star \dot{M}_* as a function of time for a counter-rotating torus of matter initially located at $R_0 = 10$. After the burst of accretion, accretion to the star continues at a small rate due to the disc's viscosity.

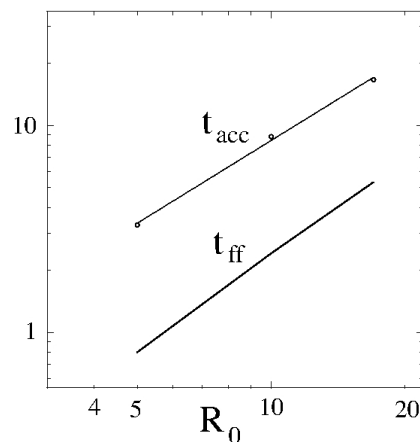


Figure 4. Accretion time t_{acc} (arbitrary scale) for torus of counter-rotating matter as a function of its initial radius $R_0 = 5, 10, 17$ and free fall times from R_0 , $t_{ff} = [2R_0^3/(9GM)]^{1/2}$.

$t_{\text{acc}}(R_0)$, can be compared to the time of free-fall $t_{\text{ff}} \approx [2R_0^3/(9GM_*)]^{1/2}$ for $R_0 \gg R_*$ for a blob of non-rotating matter to free-fall to the star. Figure 4 shows the two time scales as a function of R_0 . The accretion time-scale t_{acc} is about a factor of 3 longer than the free-fall time and it is $\propto R_0^{1.32}$. This makes sense because the free-fall time assumes that the torus is initially at rest, whereas in the simulations the torus is initially counter-rotating. The torus first loses its angular momentum to the main disc on a viscous time scale which can be estimated as $t_\nu \sim t_{\text{ff}}(Z/h)^2\alpha_\nu^{-1}$. This can account roughly for the factor of 3. Note that at the interface between the oppositely rotating components there can be a strong supersonic Kelvin-Helmholtz instability (Quach, Dyda, & Lovelace 2014) which locally increases the turbulent viscosity coefficient by a large factor.

3.2 Vertically Separated Components

Here, we consider cases where the co-rotating and counter-rotating components are vertically separated. This situation could arise from the infall of counter-rotating gas onto the surface of a preexisting co-rotating disc. That is, the disc matter at some distance above the midplane is counter-rotating with Keplerian velocity while the matter below this height is co-rotating. The fraction of the surface mass density which is counter-rotating is denoted by Δ . A conventional disc rotating in one direction has $\Delta = 0$ and a Shakura-Sunyaev accretion rate \dot{M}_{SS} which is a function of the viscosity coefficient α_ν . For $\Delta > 0$ the mass accretion rate is normalized by the value for $\Delta = 0$. That is, $\dot{m} \equiv \dot{M}_*/\dot{M}_{SS}$ for the same α_ν values. A summary of results for these runs is shown in Table 1. The most likely physical cases are those with $\Delta \ll 1$. The case $\Delta = 0.5$ is of interest because it allows comparison with the analytic solution of Lovelace and Chou (1996).

For $\Delta > 0$, a shear layer forms between the co- and counter-rotating components. Due to the viscosity, the angular momentum of the counter-rotating matter is lost to the co-rotating matter. In effect, the angular momenta of the two components is annihilated. The matter with zero angular momentum then accretes to the star with approximately free-fall speed. Figure 5 shows the behavior for $\Delta = 0.01$. After some time all counter-rotating matter has exchanged angular momentum with the main disc, and has accreted onto the star (left-hand panel). This excites disc oscillations and the system continues to evolve (right-hand panel). Notice that this small mass fraction of counter-rotating matter excites large amplitude axisymmetric warping of the main disc. Large amplitude warping was found in the earlier axisymmetric simulations by Kuznetsov et al. (1999).

We measure the peak mass accretion rate to the star $(\dot{M}_*)_p$ and the peak mass accretion rate normalized to the rate for a standard accretion disc $(\dot{m})_p$. For $\Delta \leq 0.1$ we indicate the time t_w for which all the counter-rotating matter has accreted onto the star. Figure 6 shows the logarithm of the mass accretion rate to the star as a function of time for different Δ values. Figure 7 shows on a linear scale the mass accretion rate as a function of time for $\Delta = 0.01$.

For $\Delta \leq 0.1$, there is an initial period of rapid accretion during which angular momentum is exchanged between the

counter-rotating layer and the main part of the disc. The mass accretion rate peaks at a rate $(\dot{M}_*)_p$ of $10^2 - 10^4$ times larger than the accretion rate of a conventional disc rotating in one direction. After the counter rotating matter is accreted, the accretion rate drops down to the value of conventional disc.

The duration of the period of enhanced accretion t_w does not depend significantly on the amount of counter-rotating matter. Also, it does not depend on the viscosity of the disc. This supports the conclusion that a layered counter-rotating system of initial radius R will be transient, existing only on the free-fall time scale $t_{\text{ff}} \sim R^{3/2}/\sqrt{GM}$. This is consistent with our simulation results for a counter rotating torus.

As a consistency check that our results are not due to some asymmetry in our code, the $\Delta = 0.01$ run was repeated with counter rotating layers both above and below the equatorial plane. This result is included above, indicated by an asterisk, and we see that inclusion of the second layer simply doubles the amount of matter accreting onto the star but does not change the accretion time. The reported shear layer thicknesses are the average of the upper and lower shear layers. We note that the layers thickness grows slightly more slowly, but by $t = 15$ has reached the same thickness as with the single layer case. This is likely due to the pressure from the opposite shear layer. This pressure is responsible in the single layer case for the rising of the shear layer. In this case, it acts to compress the opposite shear layer and slow its growth.

The thickness of the shear layer is determined by the angular momentum transfer rate between the counter-rotating components and by the angular momentum required for that matter to begin to free fall. For larger counter-rotating mass fractions, the growth rate of the layer thickness is smaller as more angular momentum is required to slow the layer down. Increasing the viscosity increases the rate of angular momentum transfer and hence the thickness of the layer. Note that the case $\Delta = 0.5$ can be compared with the analytic self-similar solution of Lovelace and Chou (1996) which predicts a shear layer thickness $\Delta Z \propto \sqrt{\alpha_\nu}$. Figure 8 shows the radial and angular velocity profiles as a function of Z at different radii at $t = 15$ for $\Delta = 0.5$. The shear layer thickness $\Delta Z(R)$ is taken to be the full width at half maximum of the radial velocity profiles. We find $\Delta Z \propto \alpha_\nu^{0.59 \pm 0.03}$ as shown in Figure 9. There is reasonable agreement between the theory and simulations even though the theoretical model is independent of time. A similar analysis for the $\Delta = 0.01$ case gives $\Delta Z \propto \alpha_\nu^{0.42 \pm 0.08}$. This suggests that the steady state behaviour of the shear layer is largely insensitive to the mass fraction of the counter-rotating layer.

For $\Delta = 0.5$, Lovelace and Chou (1996) also predicted the ratio of mass accretion rates of the counter-rotating disc to the standard Shakura-Sunyaev rate and found $\dot{m} = \dot{M}_*/\dot{M}_{SS} \sim (R/h)^2\alpha_\nu^{-1/2}$. Our mass accretion rates for counter rotating discs are time dependent, so that we tried accretion rates at various times and found the results to be largely insensitive to the time chosen. Figure 10 shows the data and the power law fit which gives $\dot{m} \propto \alpha_\nu^{-1.33}$. This dependence is insensitive to whether we fit to the peak mass accretion rate or the time averaged ac-

| Δ | α_ν | $(\dot{M}_*)_p$ | $(\dot{m})_p$ | M_T | t_w | $\Delta Z(R)$ | | | | | | |
|----------|--------------|-----------------|---------------|---------|-------|----------------|------|------|------|------|------|------|
| | | | | | | $t =$ $R =$ | 5 | 10 | 15 | 5 | 10 | 15 |
| 0.01 | 0.03 | 236 | 23,600 | 5,000 | 50.0 | | 0.45 | 0.56 | 0.56 | 0.77 | 1.15 | 1.38 |
| | 0.1 | 144 | 758 | 2,030 | 38.6 | | 0.85 | 1.06 | 1.36 | 1.56 | 2.18 | 2.11 |
| | 0.2 | 68.4 | 79.5 | 1,040 | 45.2 | | 1.02 | 1.29 | 1.85 | 2.15 | 2.67 | 2.43 |
| | 0.3 | 26.1 | 13.4 | 460 | 39.3 | | 1.12 | 1.46 | 1.69 | 2.30 | 3.06 | 2.46 |
| 0.02* | 0.1 | 288 | 1,516 | 4,400 | 40.0 | | 0.77 | 0.98 | 1.14 | 1.55 | 2.19 | 2.11 |
| 0.1 | 0.1 | 1,406 | 7,400 | 31,300 | 49.0 | | 0.58 | 0.70 | 0.85 | 0.78 | 1.46 | 1.86 |
| 0.5 | 0.03 | - | - | 602,700 | - | | 0.19 | 0.31 | 0.41 | 0.28 | 0.59 | 0.83 |
| | 0.1 | - | - | 260,000 | - | | 0.37 | 0.60 | 0.75 | 0.50 | 1.17 | 1.65 |
| | 0.2 | - | - | 32,590 | - | | 0.60 | 0.91 | 1.14 | 0.86 | 1.92 | 2.56 |
| | 0.3 | - | - | 15,560 | - | | 0.84 | 1.19 | 1.47 | 1.24 | 2.66 | 3.42 |

Table 1. Summary of results for vertically separated components for different counter-rotating mass fractions Δ and viscosity coefficients α_ν . The asterisk indicates symmetric wedges above and below the midplane. We measure the peak mass accretion rate $(\dot{M}_*)_p$, peak mass accretion rate normalized to a Keplerian disc $(\dot{m})_p$, the total mass accreted while there is a counter-rotating component M_T and the time required for all counter-rotating matter to accrete t_w . For times $t = 5$ and $t = 15$ we measure the thickness of the shear layer $\Delta Z(R)$, at radii $R = 5, 10, 15$.

cretion rate. The dependence on α_ν is much stronger than predicted by Lovelace and Chou (1996).

The viscous stress term $\tau_{ZR} \propto -\partial v_R / \partial Z$ in equation (5) is found to have an essential role in the counter rotating disc flows. Without this term the shear layer thickness in some cases is artificially thin and set by the grid resolution.

3.3 Radially Separated Components

an inner corotating Keplerian disc and an outer counter-rotating Keplerian disc relevant to the “Evil Eye” galaxy NGC 4826 (Braun et al. 1994; Rubin 1994b) although the galaxy’s rotation curve is not Keplerian. The top left-hand panel of Figure 11 shows the initial disc which has a jump discontinuity in the rotation direction at $R_c = 10$. Although the disc is in mechanical equilibrium, a gap rapidly forms between the co- and counter-rotating components (top right-hand panel). Owing to the viscosity there is mixing of the two oppositely rotating components. The angular momenta of the components of the mixed gas is annihilated so that the centrifugal force vanishes. This gas then falls inward towards the disc’s center. As a result the outer radius of the inner co-rotating disc begins to oscillate as matter piles up on the inner edge of the gap (bottom left-hand panel). These oscillations damp and the gap begins to fill as matter from the counter-rotating disc moves inward due to the viscosity (bottom right-hand panel).

Figure 12 shows the oscillations of the outer radius of the inner disc $R_{in}(t)$ for different values of R_c . The angular frequency of the oscillations ω_R can be compared with the radial epicyclic frequency (which for a Keplerian disc is the same as Ω_K) evaluated at average value of $R_{in}(t)$, \bar{R} . For $R_c = 5, 10, 15$, we find $\omega_R / \bar{\kappa} = 1.37, 1.56$. and 1.91 , respectively.

In addition to the oscillations of R_{in} , the inner and outer edges of the gap slowly move inward due to viscosity. Figure 13 shows this inward motion for different values of

the viscosity coefficient α_ν . The inward motion is enhanced at larger viscosities, but the frequency of the radial oscillations does not change significantly.

We find that the average mass accretion rates to the star are ~ 25 times larger than that of a conventional disc rotating in one direction with the same viscosity. This can be understood qualitatively as follows. The contact of the oppositely rotating components leads to the annihilation of the angular momenta of the mixed gas. This non-rotating gas then tends to free-fall towards the star by moving over the surface of the inner disc. As it moves inward it excites the radial oscillation of the inner disc shown in Figures 12 and 13. The increased accretion rate is largely independent of the initial position of the counter-rotating boundary. Moving the boundary from $R_c = 10$ to $R_c = 15$ increases the mass accretion rate by a factor of 1.3.

4 CONCLUSION

Observations of galaxies and models of accreting systems point to the occurrence of counter-rotating discs. Such discs may arise from the accretion of a counter-rotating gas onto the surface of an existing co-rotating disc or from the addition of counter-rotating gas at the outer radius of the existing disc. Axisymmetric 2.5D hydrodynamic simulations have been used to study two main cases – one where the oppositely rotating components are vertically separated and the other where they are radially separated. The simulations incorporate an isotropic α -viscosity including all of the terms in the viscous stress tensor including the important term τ_{RZ} . Near the interface, the two components mix and their angular momenta annihilate. This mixed gas has no centrifugal support and consequently tends to free-fall toward the star.

For vertically separated components we investigated a range of mass fractions Δ in the counter-rotating component. The simulations indicate that the counter-rotating

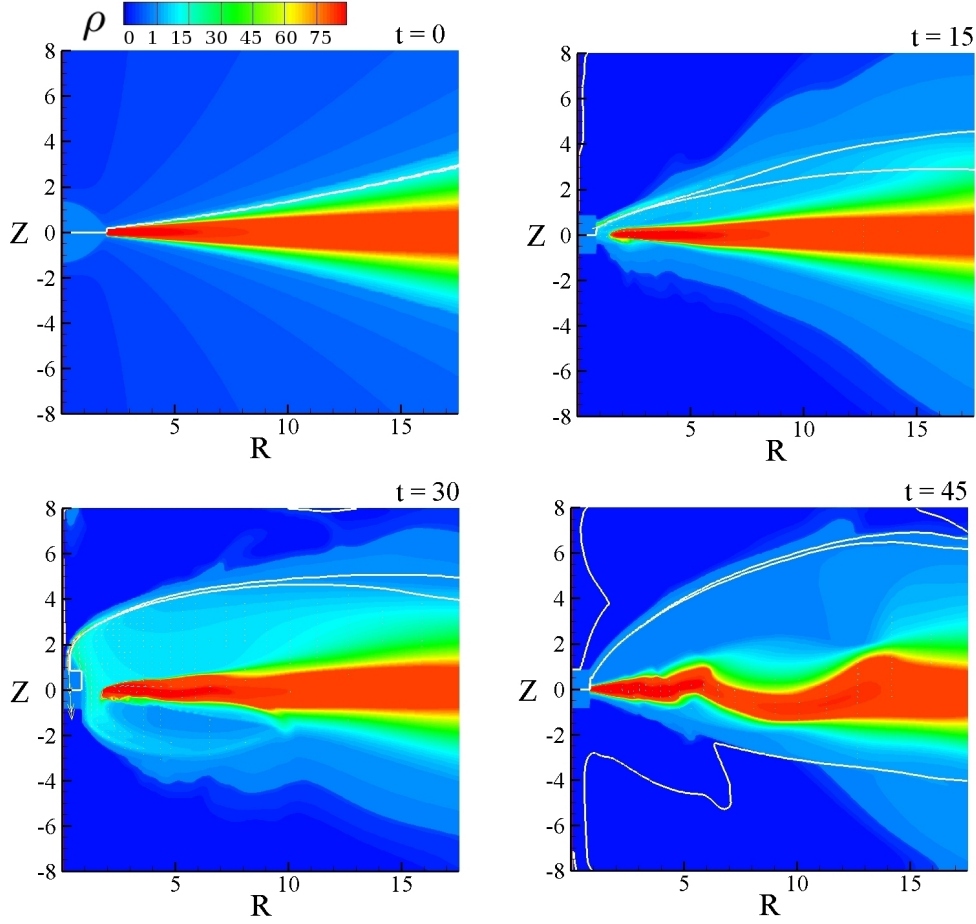


Figure 5. Density ρ (color) and angular velocity $\Omega = \pm 0.01$ contours (white lines) for $t = 0, 15, 30, 45$ for the case $\Delta = 0.01$ and $\alpha_\nu = 0.1$. The initial counter rotating layer in the upper half plane (top left-hand panel), the shear layer accretes to the star (top right-hand panel), moving upwards (bottom left-hand panel) before all counter-rotating matter has lost its angular momentum to the main disc and oscillations are induced in the disc (bottom right-hand panel). Notice the large amplitude axisymmetric warping induced in the disc.

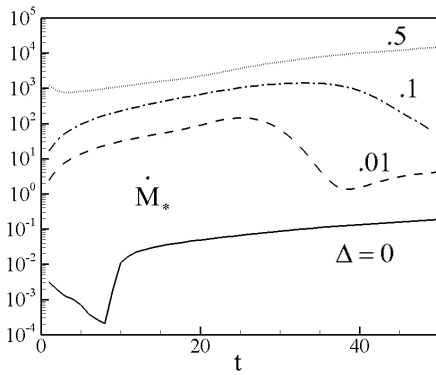


Figure 6. Mass accretion rate \dot{M}_* as a function of time t for mass fractions $\Delta = 0, 0.01, 0.1, 0.5$ and viscosity coefficient $\alpha_\nu = 0.1$.

matter extending out to a radius R accretes to the star on a time-scale about three times the free-fall time from this radius independent of Δ . The factor of three is likely due to the time required for the mixing of the two components.

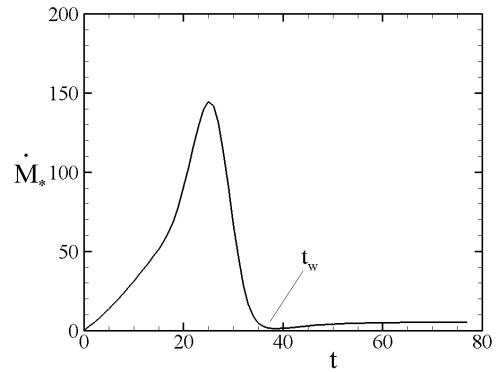


Figure 7. Mass accretion rate to the star \dot{M}_* as a function of time for $\Delta = 0.01$ and $\alpha_\nu = 0.1$. Here, t_w indicates the time at which all counter-rotating matter has accreted onto the star.

The accretion rate to the star can be enhanced by factors 10^2 to 10^4 over the rate for a disc rotating in one direction with the same viscosity. Such a burst of accretion could lead

to a comparably enhanced burst of a magnetically driven jet (e.g., Lii et al. 2012). Future investigation of counter-rotating systems including a large scale magnetic field may confirm this.

The presence of a counter rotating layer is observed to excite a large amplitude axisymmetric warp in the disc similar to the warping observed in the earlier study by Kuznetsov et al. (1999). For the case where the two components have the same mass the simulation results are compared with the analytic self-similar solution of Lovelace and Chou (1996). The dependence of the shear layer thickness on the viscosity agrees approximately with this theory but not with predicted mass accretion rate dependence on viscosity.

For the case of radially separated components we observed a more modest increase by a factor ~ 25 in the accretion rate over that of a conventional disc. The mixed gas

at the interface tends to fall inward and this is observed to excite radial oscillations of the inner disc with a frequency of the order of the radial epicyclic frequency. This enhanced accretion is significant for the King and Pringle (2006, 2007) picture of massive black hole accretion discs built up from a sequence of clouds with random angular momenta which gives a disc with rotation direction alternating as a function of radius.

Important future work will be full 3D hydrodynamic simulations including the heating, cooling, and radiative transfer of the gas of counter-rotating discs. This will account for the supersonic Kelvin-Helmholtz instability, which is a 3D instability, as well as the strong shocks which it induces (see Quach et al. 2014). The time-scale of mixing of the two components and their loss of angular momentum is expected to be shortened compared with the present results.

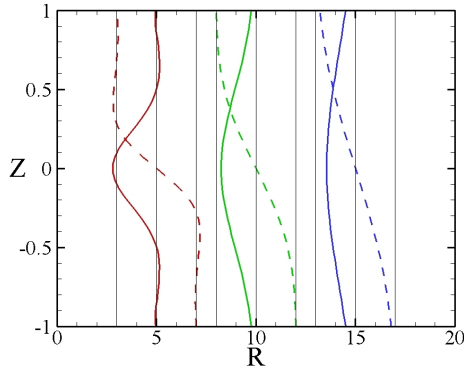


Figure 8. Radial and angular velocity profiles as a function of Z $v_r(R, Z)$ (solid curves) and $\Omega(R, Z)$ (dashed curves) at radii $R = 5$ (red), 10 (green) and 15 (blue) in units of the local Keplerian velocity and angular velocity (indicated by the vertical lines) for the case $\Delta = 0.5$, $\alpha_\nu = 0.1$ at $t = 15$. The velocity profiles are approximately Gaussian and peaked at $Z = 0$ where $\Omega = 0$.

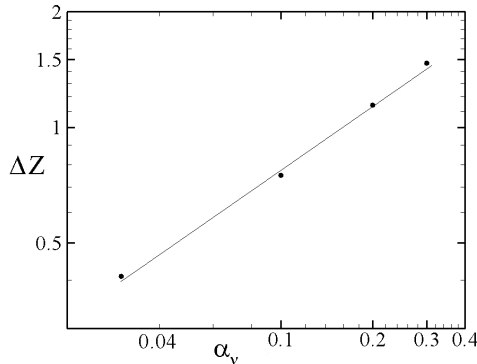


Figure 9. Full width at half-maximum of the radial velocity distribution $\Delta Z(R)$ as a function of viscosity α_ν for $R = 15$ and $t = 15$ for the case $\Delta = 0.5$. The fit for radii $R = 5, 10, 15$ and $t = 5, 15$ gives a power law dependence $\Delta Z \propto \alpha_\nu^{0.59 \pm 0.03}$, in general agreement with the self-similar solution $\Delta Z \propto \sqrt{\alpha_\nu}$ of Lovelace and Chou 1996).

ACKNOWLEDGMENTS

This work was supported in part by NASA grants NNX11AF33G and NSF grant AST-1211318.

REFERENCES

- Alig, C., Schartmann, M., Burkert, A., & Dolag, K. 2013, ApJ, 771, 119
- Braun, R., Walterbos, R.A.M., Kennicutt, R.C., Tacconi, L.J., 1994, ApJ, 420, 558
- Chakrabarty, D., Bildsten, L., Finger, M. H., Grunsfeld, J. M., Koh, D. T., Nelson, R. W., Prince, T. A., Vaughan, B. A., & Wilson, R. B. 1997, ApJ, 481, L101
- Choudhury, S., Lovelace, R.V.E., 1983, ApJ, 283, 331
- Ciri, R., Bettoni, & Galletta, G. 1995, Nature, 375, 661
- Comins, N.F., Lovelace, R.V.E., Zeltwanger, T., & Shorey, P. 1997, ApJ, 484, L33
- Corsini, E.M. 2014, in *Counter-Rotation in Disk Galaxies*, ASP Conference Series, Vol. 486, Eds. E. Iodice & E. M. Corsini (ASP: San Francisco), p. 51
- Galletta, G. 1996, in *Barred Galaxies*, IAU Colloq. 157, Eds. R. Buta, D. Crocker, & B. Elmegreen, ASP Conference Series, 91, 11
- Gulati, M., Tarun, D.S., & Sridhar, S. 2012, MNRAS, 424, 348
- King, A.R., & Pringle, J.E. 2006, MNRAS, 373, L90
- King, A.R., & Pringle, J.E. 2007, MNRAS, 377, L25
- Kuznetsov, O. A., Lovelace, R. V. E., Romanova, M. M., & Chechetkin, V. M. 1999, ApJ, 514, 691
- Li, L., & Narayan, R., 2004, ApJ, 601, 414
- Lii, P., Romanova, M.M., & Lovelace, R.V.E. 2012, MNRAS, 420, 202
- Lovelace, R.V.E., & Chou, T., 1996, ApJ, 468, L25
- Lovelace, R.V.E., Jore, K.P., & Haynes, M.P. 1997, ApJ, 475, 83
- Nelson, R. W., Bildsten, L., Chakrabarty, D., Finger, M. H., Koh, D. T., Prince, T.A., Rubin, B. C., Scott, D. M., Vaughan, B. A., & Wilson, R. B. 1997, ApJ, 488, L117
- Nixon, C.J., King, A.R., Price, D.J., 2012, MNRAS, 422, 2547
- Quach, D., Dyda, S., & Lovelace, R.V.E. 2014, MNRAS, submitted
- Ray, T.P. 1981, MNRAS, 196, 195
- Ray, T.P. 1982, MNRAS, 198, 617
- Remijan, A.J., & Hollis, J.M. 2006, ApJ, 640, 842
- Rubin, V.C., Graham, J.A., Kenney, J.D.P. 1992, ApJ, 394, L9
- Rubin, 1994, AJ, 107, 173
- Rubin, 1994, AJ, 108, 456
- Lii, P., Romanova, M.M., & Lovelace, R.V.E. 2012, MNRAS, 420, 2020
- Sage, L.J., & Galletta, G., 1994, ApJ, 108, 1633S.
- Shakura, N.I., & Sunyaev, R.A. 1973, A&A, 24, 337
- Tang, Y.W., Guilloteau, S., Pietu, V., Dutrey, A., Ohashi, N., & Ho, P.T.P., 2012, A & A, 547, A84
- Vorobyov, E.I., Lin, D.N.C., & Guedel, M. 2014, A&A, in press

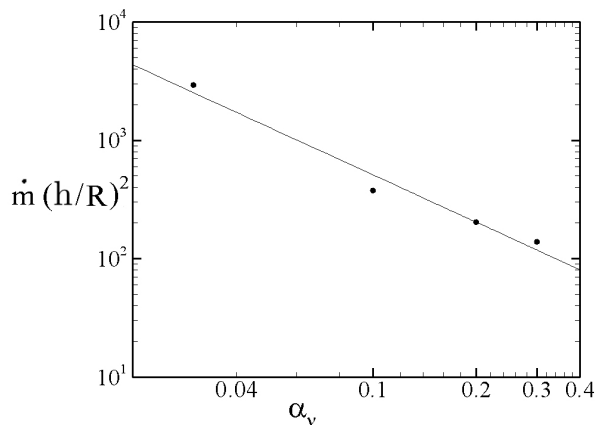


Figure 10. Mass accretion rate to the star as a function of the viscosity coefficient α_ν for $\Delta = 0.5$. The fit yields a power law dependence of $\dot{m} \propto (R/h)^2 \alpha_\nu^{-1.33 \pm 0.03}$, in disagreement with the self-similar solution $\dot{m} \propto (R/h)^2 \alpha_\nu^{-1/2}$ of Lovelace and Chou (1996).

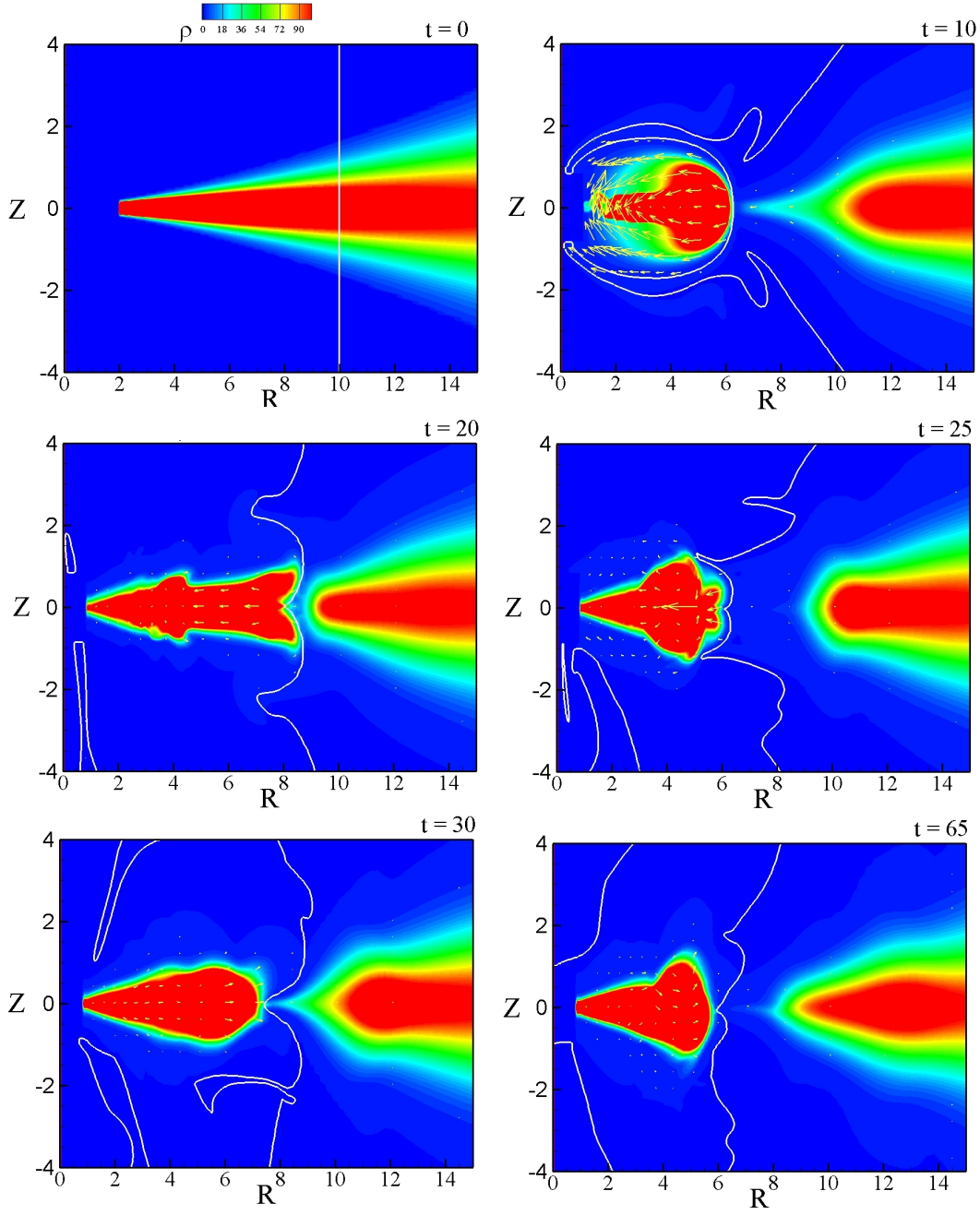


Figure 11. Plot of density ρ (color) and angular velocity $\Omega = 0$ contour (white line) for $t = 0, 10, 20, 25, 30, 65$. The initial radius of the boundary between the co- and counter-rotating components $R_c = 10$. A gap rapidly opens in the disc layer due to the mixing of the two components. This in turn excites a radial, axisymmetric breathing mode. Subsequently, the inner disc oscillates quasi-periodically.

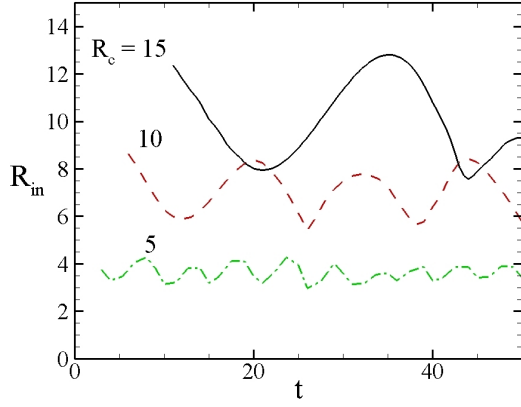


Figure 12. Outer radius of the inner disc as a function of time for initial counter-rotating boundary at $R_c = 5, 10, 15$. The frequency of the oscillations is approximately the radial epicyclic frequency at the average value of R_{in} .

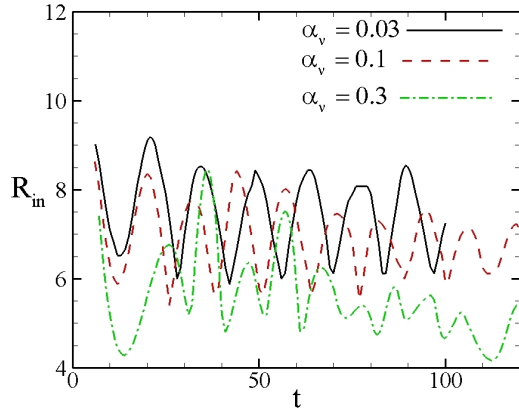


Figure 13. Outer radius of the inner disc as a function of time for initial counter-rotating boundary at $R_c = 10$ and viscosity coefficients $\alpha_v = 0.03, 0.1, 0.3$. The frequency is only weakly dependent on the disc viscosity. Increasing disc viscosity causes the minima of the oscillations to decrease more rapidly. The amplitude of the oscillations also decreases.